JOURNAL OF SYNCHROTRON RADIATION

ISSN 1600-5775

Received 13 August 2015
Accepted 26 October 2015

Edited by S. Svensson, Uppsala University, Sweden

Keywords: X-ray waveguides; capillary optics; microchannel plate; X-ray fluorescence propagation; X-ray spectroscopy.

Excitation and propagation of X-ray fluorescence through thin devices with hollowed ordered structures: comparison of experimental and theoretical spectra

M. I. Mazuritskiy,[a] S. B. Dabagov,[b,c,d] A. Marcelli,[b,e]* A. M. Lerer[a] and K. Dziedzic-Kocurek[f]

[a]Physics Department, Southern Federal University, Rostov-on-Don, Russia, [b]INFN Laboratori Nazionali di Frascati, 00044 Frascati, Italy, [c]RAS PN Lebedev Physical Institute, Moscow, Russia, [d]NR Nuclear University MEPhI, Moscow, Russia, [e]RICMASS, Rome International Center for Materials Science Superstripes, Via dei Sabelli 119A, 00185 Rome, Italy, and [f]M. Smoluchowski Institute of Physics, Jagiellonian University, Krakow, Poland.
*Correspondence e-mail: marcelli@lnf.infn.it

The lack of models describing the propagation of X-rays in waveguides and the interference mechanism between incident and reflected radiation waves hamper the understanding and the control of wave propagation phenomena occurring in many real systems. Here, experimental spectra collected at the exit of microchannel plates (MCPs) under the total X-ray reflection condition are presented. The results are discussed in the framework of a theoretical model in which the wave propagation is enhanced by the presence of a transition layer at the surface. The angular distributions of the propagating radiation at the exit of these MCPs with microchannels of ~3 μm diameter will also be presented and discussed. These spectra show contributions associated with the reflection of the primary monochromatic beam and with the fluorescence radiation originating from the excitation of atoms composing the surface of the microchannel. The soft X-ray fluorescence spectra collected at the exit of microcapillaries were analyzed in the framework of a wave approximation while diffraction contributions observed at the exit of these hollow X-ray waveguides have been calculated using the Fraunhofer diffraction model for waves in the far-field domain. Data collected at the Si *L*-edge show that in glassy MCPs the fluorescence radiation can be detected only when the energy of the primary monochromatic radiation is above the absorption edge for grazing angles higher than half of the critical angle of the total reflection phenomenon. Experimental data and simulations of the propagating radiation represent a clear experimental confirmation of the channeling phenomenon of the excited fluorescence radiation inside a medium and point out that a high transmission can be obtained in waveguide optics for parameters relevant to X-ray imaging.

1. Introduction

Capillary optics is one of the fastest growing optical technologies, in particular because of its superior capacity of generating high-flux-density X-ray beams in the micrometer and sub-micrometer range (Pfeiffer *et al.*, 2002; Sun *et al.*, 2009; Dabagov, 2003). Properties and peculiarities of X-ray beams formed by polycapillary optics have been investigated since the 1990s (Kumakhov, 1990; Bilderback *et al.*, 1994; Dabagov *et al.*, 1995; Bukreeva *et al.*, 2010; Salditt *et al.*, 2008). Nowadays, the characterization of X-ray waveguides and microcapillary optics based on the phenomenon of multiple total external reflections is devoted to ultra-focusing properties and

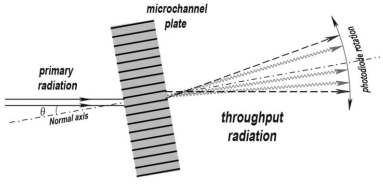

to the control of partially coherent beams. Actually, because the technology based on the capillary optical elements may, in principle, deliver a high flux density within a sub-micrometer spot, its understanding is mandatory for developing novel optical systems or for optimizing existing applications. Indeed, optimized capillary-based systems would be capable of increasing the radiation density and eventually of shaping X-ray beams replacing in many optical layouts the long optical focusing devices used at present. Furthermore, the use of waveguides for spatial and spectral filtering may allow decoupling radiation beam and source properties. Actually, channeling-based devices may guide and shape an X-ray beam and control intensity, spot size, divergence and spatial distribution.

Being large and effective low-weight optics, microchannel plates (MCPs) have already been used for low-power instruments for different technical developments and scientific applications (Zhang *et al.*, 2014). They are very flexible devices, and applications also include telescopes. Arrays of MCPs may collectively provide a wide angle of view for X-ray imaging in the energy range from a few tens of eV to a few keV (Pavlinsky *et al.*, 2006). Moreover, their characteristics make them suitable as focusing lenses for excited radiation, and, due to their broad-band, also for microbeam X-ray fluorescence, scanning microscopy or as filters (Tsuji *et al.*, 2004; MacDonald, 2010).

The propagation features inside a microchannel are defined by the interaction of the radiation with the waveguide surface and characterized in terms of waves propagating close to capillary walls. A fundamental issue of the X-ray beam transport inside capillary channels is the mode regime (Dabagov *et al.*, 2000; Dabagov, 2003; Bukreeva *et al.*, 2010; Salditt *et al.*, 2008) and, in particular, that associated with the surface channeling of the X-ray radiation.

Although the channeling of X-rays through a capillary system is a complex phenomenon depending on optical layout, capillary parameters, radiation properties, *etc.*, whose knowledge is still a matter of debate, the application of wave optics methods allows the guided propagation mechanism of X-ray radiation to be described.

At present, experimental investigations of X-ray transmission through microcapillary structures, aimed at the R&D of dedicated optics working in the 'water window' spectral region, are limited. Previous studies (Mazuritskiy, 2006, 2012; Mazuritskiy *et al.*, 2013*a*,*b*, 2014, 2015) were devoted to the characterization of the propagation of radiation hitting the walls inside the hollow channel of a MCP, and how the excited fluorescence radiation can be transported by MCP polycapillary structures. In the following sections we will show and discuss synchrotron radiation spectral data and the angular distribution of the intensity collected at the exit of MCPs. In particular, we will analyse the low-energy inelastic scattering experiments in the region of the anomalous dispersion above and below the Si *L*-edge and compare data with theoretical calculations taking into account the presence of a transition layer below the wall surface.

2. Experimental set-up

The layout shown in Fig. 1 describes the experimental optical configuration based on the polarimeter end-station (Shafers *et al.*, 1999) installed on the UE56-SGM beamline of the BESSY II synchrotron radiation facility. Fig. 1(*a*) shows the layout of the rotational alignment of the photodiode at the exit of the MCP, while Fig. 1(*b*) shows the rotational geometry of the MCP for each position of the photodiode. In the transmission geometry in Fig. 1(*b*) the grazing angle θ between the incident primary beam and the microchannel walls of the MCP may change while rotating the MCP around the 'θ' axis.

We performed experiments using MCPs with a thickness of $\sim$0.3 mm made of lead silicate ($PbSiO_3$). These devices, manufactured by BASPIK (Vladikavkaz Technological Center; http://www.baspik.com/eng/products/nauka/), present in the transverse cross section a hexagonal pattern of pores with a diameter of 3.4 µm and a pitch size of 4.2 µm. The top surface of the MCP is illuminated from the left-hand side (as shown in Fig. 1) by a monochromatic beam with a divergence of <5 mrad. Then, the radiation propagating inside the MCP microchannels is collected by a photodiode with a diaphragm of 200 µm diameter placed on the entrance side of the device. Data have been collected using a beam size of 60 µm × 60 µm and the distance between the sample and the window of the photodiode was set to 145 mm. After we identified the 'zero angle' position of the polarimeter, *i.e.* the angle for which the primary beam hits the center of the photodiode detector without the MCP [XX' direction in Fig. 1(*b*)], the angular distributions [Fig. 1(*a*)] were measured for different angles of the detector with respect to the MCP.

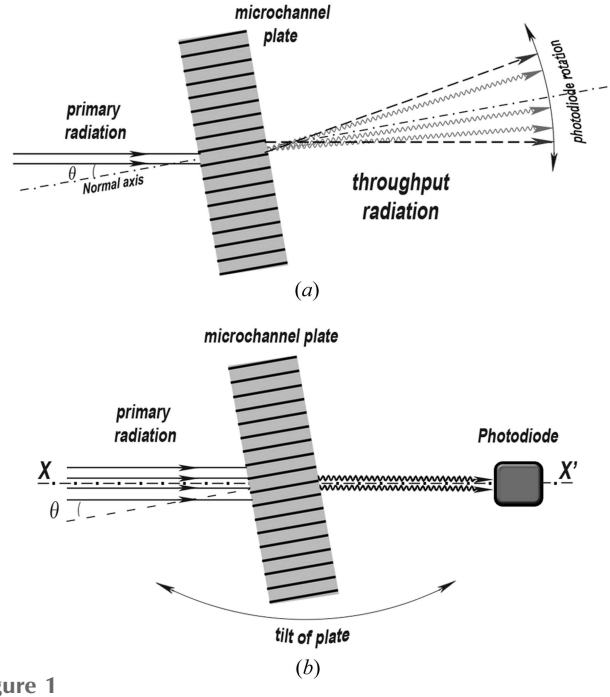

Figure 1
Optical layouts of the MCP transmission-based experiments using the polarimeter station at BESSY II.

We assumed that the microchannel walls were oriented parallel to the normal of the MCP surface. Inserting the MCP along the radiation path, the 'normal' direction to the MCP surface corresponds to the relative 'zero angle' position of the measured angular scan. After setting the grazing angle θ of the polarimeter, the angular distributions of the radiation behind the MCP are collected scanning the detector angle. In Fig. 1(*a*) the dash-dot line is the 'zero' direction, *i.e.* the direction parallel to the walls.

We measured the angular distribution of the radiation at the exit of the MCP, *i.e.* intensity *versus* angle, under the total external reflection condition for different grazing angles of the incident beam. The angular scans of the detector (*versus* angle 'φ' of the photodiode) show the positions where the maximum intensity of the emitted radiation occurs. We measured, for different values of the θ angle, *i.e.* the angle between the incident monochromatic radiation and the MCP microchannel walls, the intensity distribution between the two maxima occurring at $\varphi = \pm\theta$ in the angular range $-\theta \leq \varphi \leq \theta$. Moreover, we also collected energy spectra at different θ angles, and at different angles $\varphi_1, \varphi_2, \varphi_3, \ldots, \varphi_n$ of the photodiode.

3. Method

3.1. Theoretical model

The theoretical framework we considered to reproduce the experimental data discussed in the following section is based on the following approximations:

(i) A constant propagation and a constant attenuation (excitation) of wave modes inside a single capillary structure.

(ii) The wave parameters of a single capillary are the same as for a MCP polycapillary device.

(iii) The amplitudes at the entrance of a polycapillary are obtained using the Kirchhoff–Huygens method.

(iv) The mode amplitudes are calculated, using the attenuation (excitation) parameters, at the exit of a capillary.

(v) The angular distribution of the X-ray radiation at the exit of a MCP has been calculated using the Kirchhoff–Huygens method.

(vi) X-ray diffraction patterns at a long distance from a MCP have been calculated using the Fraunhofer diffraction model for propagating waves.

In addition, we took into account a small polarization of X-ray waves in the waveguide ($|\varepsilon| \cong 1$) and the field is described with a scalar potential,

$$\Psi(r, \varphi, z) = U(r)\cos m\varphi \exp(-i\gamma z),$$

where γ is the complex propagation constant. The function $\Psi(r, \varphi, z)$ has to satisfy the Helmholtz equation

$$\Delta\Psi(r, \varphi, z) + k^2\varepsilon(r)\Psi(r, \varphi, z) = 0,$$

where Δ is the Laplace operator, $k = 2\pi/\lambda$ and λ is the radiation wavelength in a vacuum. Moreover, the inner surfaces of the microchannels have been approximated in terms of a cylindrical transition layer made by N sub-layers, *i.e.* N cylinders with different radii. The permittivity of each cylinder is constant and can be approximated by the dielectric constant of the cylindrical layer between the surface and the bulk (Mazuritskiy *et al.*, 2015). The dispersion equation for the complex value of the propagation constant γ has been numerically solved as previously described (Lerer *et al.*, 2014).

3.2. Calculation of parameters for waveguide modes in a single capillary

X-ray radiation propagates through silicon glass plates in a vacuum inside an empty cylindrical waveguide (pore). Taking care of the different parameters, including those associated with the manufacture technology, the influence of moisture and air, the chemical elements concentration profile and the surface density, the physical chemical properties of the transition layers are a function of the depth (Fechtchenko *et al.*, 2000; Feranchuk *et al.*, 2007). Actually, soft X-rays interact with a substance at the surface, where the spatial permittivity profile has to be considered. The MCPs we measured are made by a lead silicate whose internal pores have been treated and can be described as a superposition of different layers going from the surface to the inner side. According to that, the internal wall can be described as made by a surface that can be described in terms of the permittivity ($\varepsilon \approx 1 - \delta - i\beta$).

3.3. Calculation of the mode amplitudes at the entrance of a capillary

We may now consider the propagation of plane waves in a system of coordinates $z = 0$, $z = -h$ corresponding to the entrance and the exit of a waveguide, respectively. The equation below describes a plane wave at the entrance of a capillary,

$$\Psi^0(x, z) = \exp\left[i\left(k_x x + k_z z\right)\right], \tag{1}$$

where $k_x = k\sin\varphi$, $k_z = k\cos\varphi$ and φ is the grazing angle between the X-ray beam and the wall of the pore. In the plane $z = 0$ we will have

$$\begin{aligned}\Psi^0(x, 0) &= \exp(ik_x x) = \exp(ik_x r\cos\varphi) \\ &= 2\sum_{m=0}^{\infty} \nu_m i^m J_m(k_x r)\cos m\varphi\end{aligned} \tag{2}$$

where $J_m(k_x r)$ is the Bessel function, and

$$\nu_m = \begin{cases} 1/2, & m = 0, \\ 1, & m \neq 0. \end{cases}$$

At the entrance of the pore the amplitude of the wave $A_{mn}(0)$ can be calculated as

$$A_{mn}(0) = \int_0^R r\,\mathrm{d}r \int_0^{2\pi} \Psi^0(r\cos\varphi, 0)\Psi_{mn}(r, \varphi, 0)\,\mathrm{d}\varphi, \tag{3}$$

and substituting equations (1) and (2) into (3) we obtain

$$A_{mn} = 2\pi\, i^m I(m, \kappa_{mn}, k_x, R),$$

$$I(m, \kappa_{mn}, k_x, R) = \int_0^R r J_m(k_x r)\, J_m(\kappa_{mn} r)\, \mathrm{d}r$$

$$= R\, \frac{\kappa_{mn} J_{m-1}(\kappa_{mn} R)\, J_m(k_x R) - k_x J_m(\kappa_{mn} R)\, J_{m-1}(k_x R)}{(\kappa_{mn})^2 - {k_x}^2},$$

where κ_{mn} is the transverse wave mode number with the indexes m and n. The amplitude at the exit of the pore is

$$A_{mn}(h) = A_{mn}(0) \exp(-\gamma''_{mn} h)$$

where $\gamma''_{mn} = \mathrm{Im}\, \gamma_{mn}$ is the attenuation coefficient in the case of $\gamma''_{mn} > 0$, and the excitation coefficient for $\gamma''_{mn} < 0$. Within this approximation, the total field inside a pore can be calculated as

$$U_\Sigma(r, \varphi, z) = \sum_{m=0}^{\infty} \sum_{n=1}^{\infty} A_{mn} U_{mn}(r, \varphi, z)$$

$$= \sum_{m=0}^{\infty} \sum_{n=1}^{\infty} A_{mn} J_m(\kappa_{mn} r) \cos m\varphi \exp(i\gamma_{mn} z). \quad (4)$$

3.4. The X-ray angular distribution at the exit of a MCP

The radiation field at the exit of a MCP can be considered as a double sum in term of spatial harmonics,

$$V(x, y, z) = \sum_{p=-\infty}^{\infty} \sum_{q=-\infty}^{\infty} B_{pq} \exp\left[i\chi_{pq}(x, y, z)\right], \quad (5)$$

where B_{pq} is the amplitude of the spatial harmonic and $\chi_{pq}(x, y, z)$ is the phase. Because of the X-ray condition $z \gg \lambda$, we performed calculations only for the waves with $k > \rho_{pq}$. The amplitudes of the spatial harmonics can be written as

$$B_{pq} = \int_0^R r\, \mathrm{d}r \int_0^{2\pi} V(x, y, h) U_\Sigma(r, \varphi, h)\, \mathrm{d}\varphi, \quad (6)$$

and substituting equations (4) and (5) into (6) we obtain

$$B_{pq} = 2\pi \sum_{m=0}^{\infty} i^m \sum_{n=1}^{\infty} A_{mn}\, I\left(m, \kappa_{mn}, \rho_{pq}, R\right). \quad (7)$$

In (7) the sum over n considers only propagating waveguide modes and the upper limit of the sum over m has been selected according to the necessary calculation accuracy. However, it usually does not exceed the value of 3. Each spatial harmonic is a plane wave whose projections of the wavevector on the 'x,y' plane are α_p, β_{qp}. The angles of the diffraction peaks (in the spherical coordinates) are defined as

$$k_{x,pq} = k \cos\varphi_{pq} \sin\theta_{pq} = \alpha_p,$$

$$k_{y,pq} = k \sin\varphi_{pq} \sin\theta_{pq} = \beta_{qp},$$

$$k_{z,pq} = k \cos\theta_{pq} = \gamma_{pq}.$$

4. Results and discussion

The angular distributions of the radiation intensity at the exit of a MCP sample, at different θ angles and different detector positions (φ angles), have been collected in transmission mode. The multiple reflection radiation distributions and the corresponding maxima in the spectra are compared in Fig. 2 where the main features of the measured angular distributions taken at the fixed grazing angle of $\theta = 3°$ for three different energies just below and above the energy of the Si L-absorption edge are shown. The distributions are substantially mirror-like with two intense specular maxima due to the reflection contributions of the primary monochromatic radiation at A ($\theta = -3°$) and A' ($\theta = 3°$). Still, the two maxima do not have the same intensity and are slightly asymmetric with a more intense A peak and an intense satellite (B). Actually, this can be due to a smaller angular asymmetry of the primary beam (see Fig. 1*a*) relative to the 'normal axis' of the MCP.

The polarimeter station also gives the possibility to set the photodiode position on each of the angular positions corresponding to the maxima A and A' shown in Fig. 2. The spectra *versus* energy collected at the exit of the MCP at $\theta = -3°$ and $\theta = 3°$ show the same fine structures as the reflection spectra previously measured with these MCPs (Mazuritskiy, 2012; Mazuritskiy, *et al.*, 2013*a*). It should be underlined that, because of their composition, the fine structures of the transmission energy spectra of our MCP samples are substantially similar to the reflection spectrum of a lead silicate glass.

In the experimental configuration we worked well below the critical angle (θ_c) because θ_c for the total reflection at the energy of the Si L-edge is $\sim 8°$. Nevertheless, as shown in Fig. 3, by increasing the grazing angle up to 5°, spectra collected for energies below and above the Si L-edge become more complex and strongly asymmetric. Moreover, although all spectra are still characterized by two almost symmetric peaks A ($\varphi = -5°$) and A' ($\varphi = 5°$) corresponding to the detector positions and due to multiple reflections of the incident radiation at the grazing angle of $\theta = 5°$, they are clearly more structured and complex.

The two maxima have the same nature as the peaks observed in the spectra collected at grazing angle $\theta = 3°$ in Fig. 2. At the same time, Fig. 3 shows three other intense

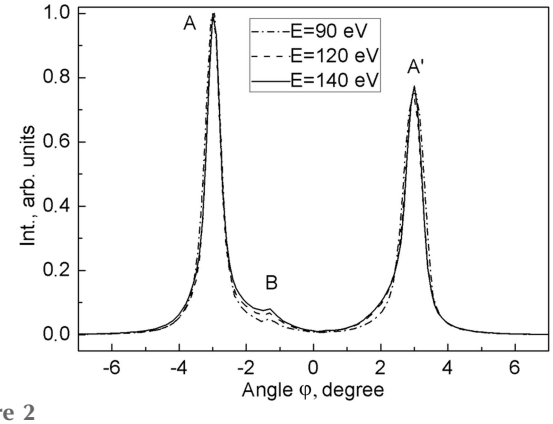

Figure 2
Angular-resolved spectra measured at the grazing angle of $\theta = 3°$ (see layout in Fig. 1) for different values of the incident radiation below and above the Si L-edge.

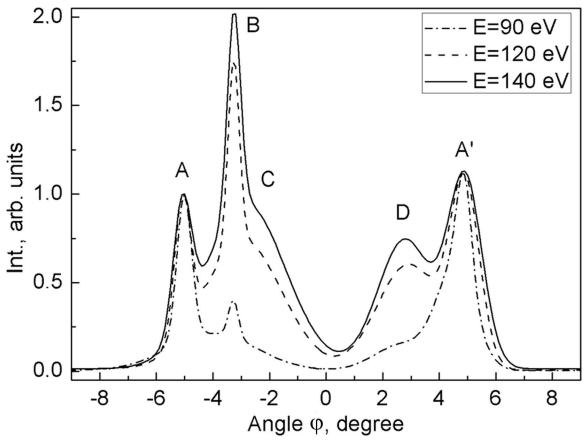

Figure 3
Angular-resolved spectra measured at the grazing angle of $\theta = 5^\circ$ (see layout in Fig. 1) for different values of the incident radiation below and above the Si L-edge.

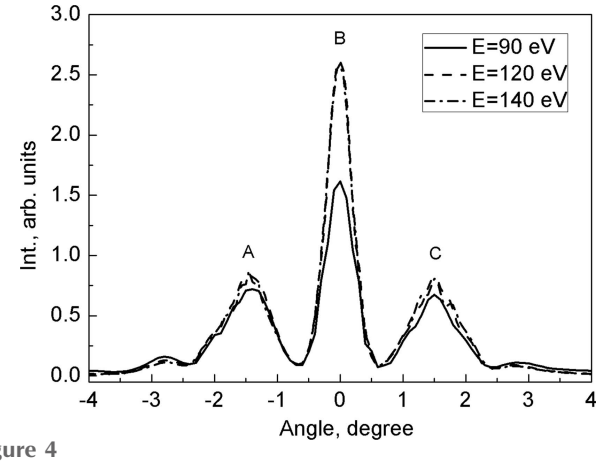

Figure 4
Angular distributions of the intensity at the exit of a MCP for different energies of the primary radiation around the Si L-edge.

structures, named B, C and D. The spectrum at the energy of 90 eV appears to be similar to those shown in Fig. 2 while those at higher energy are much different from the previous ones and are more asymmetric. In particular, peaks B and C do not have a real correspondence on the right side where only the peak D is resolved. The intensity of these features is different, but also the width of the left side structures is smaller than that on the right side of these spectra.

Peaks B, C and D clearly appear only in the spectra measured at energies higher than the Si L-edge ($\sim$100 eV). As a consequence, these structures can be associated with the excited fluorescence radiation propagating through the microchannels. Positions and intensities of the fluorescence peaks in the spectra in Fig. 2 depend on the angular position of the microchannels in the transverse cross section of the MCP relative to the direction of primary radiation. Unfortunately, the experimental layout of the polarimeter does not allow the sample to be rotated around the XX' axis (see Fig. 1b); as a consequence it is not possible to change the orientation of the microchannels of a MCP.

In Fig. 3, spectra collected at the grazing angle of $\theta = 5^\circ$ are shown with solid and dashed lines. Comparison of spectra collected at $\theta = 5^\circ$ and $\theta = 3^\circ$ indicates that at the smaller angle only two structures, corresponding to the reflected radiation, are clearly detected: peaks A and A'. Neglecting the weak feature B in Fig. 2, which is present in all spectra and probably independent of the excitation energy, the fluorescence radiation is significantly excited in the microchannels and transmitted by a MCP device only when the radiation hits the walls at a grazing angle greater then $\theta_c/2$. This experimental result, supported by the model introduced above, points out that the excitation of the fluorescence radiation at large angles (but smaller than the critical angle) occurs only at energies higher than the Si L-edge.

We also set the photodiode at the 'zero angle' position with respect to the direction of the primary radiation, measuring the angular distributions of the soft X-ray radiation propagating inside the MCP's microchannels as a function of the angle 'θ' (see Fig. 1b). Looking at the spectra in Fig. 4, we can identify three maxima: A, B and C. Differences in the fine structure of the A and C peaks in the spectra at 90 eV, 120 eV and 140 eV are related to the wave propagation of the X-ray radiation inside the microchannels at the angle of $\sim$1.5°. All spectra have been normalized to the beam current. Accordingly, the intensity of the maximum B for radiation energies above the Si L-edge (120 eV and 140 eV) is $\sim$1.5 higher than that measured below the absorption edge (90 eV). The result is clearly associated with an enhanced propagation of the fluorescence radiation along the axis of the microchannels when the excitation energy is higher than the Si L-edge (Okotrub *et al.*, 2005).

The model we proposed may describe the propagation of the fluorescence in a hollow waveguide taking into account the interaction of the primary beam at the entrance of an optical structure whose pores are described as the combined contribution of several layers. The electromagnetic field in the layer is then described as the superposition of the different modes of the plane waves travelling inside these pores at angles smaller than the critical angle of the total reflection. We used the Fraunhofer diffraction model for waves and calculated X-ray diffraction patterns at a long distance from the MCP. In Fig. 5(a) we compare the model of the angular distribution (solid line) with the experimental spectrum (dashed line) of the radiation intensity collected at the output of the MCP at the energy E = 120 eV with the experimental layout of the polarimeter (Fig. 1b). The calculations have been performed at the same energy for a MCP with pores of 3.4 µm diameter and a pitch size of 4.2 µm. Although the fine structure details of the side peaks (A, C) are broader in the calculations, both curves normalized to the intensity of the central peak B exhibit a good agreement. Theory agrees both in relative intensity and angular position. Moreover, the calculation clearly shows that a rotation of the MCP microchannels relative to the axis XX', *i.e.* the primary beam direction in Fig. 1, does not affect the shape of the spectrum shown in Fig. 5. Indeed, the experimental condition outlined in Fig. 1(b) has been set to run with a high angular resolution for the

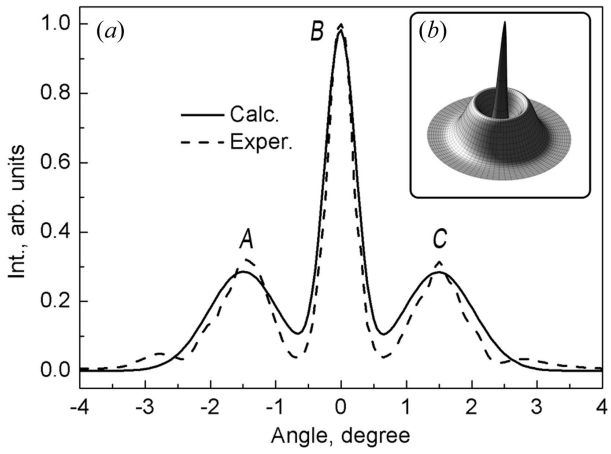

Figure 5
Experimental and theoretical curves of the angular distributions at the exit of a MCP for primary radiation at the energy E = 120 eV.

detector. The distance between the MCP and the window of the photodiode was set to 145 mm and the entrance window to 0.2 mm. Taking into account the wavelength and the structure of the MCP, the detector collected radiation corresponding to the X-ray diffraction of waves penetrating through a single capillary. In this experimental geometry, we fulfilled the axial symmetry and, as a consequence, a generic rotation of MCP microchannels relative to the axis XX' does not affect the spectral shape.

In Fig. 5(b) we show the distribution of the radiation intensity at the exit of the MCP obtained by rotating the sample around the XX' axis and changing, at the same time, the tilt angle of the primary radiation with respect to the microchannels wall in the range $-4^\circ \leq \theta \leq 4^\circ$.

5. Conclusion

In this contribution we have presented and discussed the angular distributions of the radiation in the energy range of the Si L-edge at the exit of MCPs. For these experiments we used MCPs with thin hollow regular structures made by pores of diameter $\sim$3 µm. The intensity of the radiation at the exit of such a structure has a particular angular distribution showing maxima corresponding to the transmission of fluorescence radiation excited inside these structures. The experiments are then clear evidence of the channeling phenomenon of the excited fluorescence radiation inside a real medium. If we define θ as the angle between the primary monochromatic beam and the microchannel walls, the spectra show that, for energies of the incident radiation greater than the absorption edge, fluorescence radiation contributions can be detected at the exit of a MCP when the grazing angles are greater than half of the critical angle ($\theta \geq \theta_c/2$) of the inner surface of these silicate-based devices. The transmission spectra measured at the exit of MCPs are then the superposition of reflection and fluorescence contributions propagating inside the MCPs.

The theoretical model we introduced demonstrates that waves penetrating inside the pores modify the wavefield at the internal surface of a pore with a significant increase of the energy flux transmitted by the MCP. Moreover, an additional spatial modulation of the electromagnetic field at the exit of these structures is observed. Actually, these experiments combined with simulations may allow the optimal transport conditions for the excited fluorescence radiation inside a microcapillary to be identified or a large set of microcapillaries such as a MCP device.

The experiments also allow the improvement of models describing the propagation of soft X-ray radiation in a hollow waveguide and the interference between incident and reflected (fluorescence) waves. Data indeed represent unique information on the wave propagation phenomenon, extremely useful for many foreseen applications, in particular those associated with the use of coherent X-ray sources (Dabagov *et al.*, 2000; Dabagov & Marcelli, 2000). Combining experimental data and accurate calculations we may better understand and clarify the channeling phenomenon at soft X-ray energies. Moreover, the results we presented, in particular the angular dependence, could be extremely useful for the development of X-ray microfluorescence spectrometers for fast collection of complex chemical compositions or to avoid the scanning procedure probing the elemental distribution of relatively large samples.

Acknowledgements

We would like to thank A. Gaupp, A. Sokolov and F. Schäfers for assistance during experimental runs at BESSY and many critical discussions. This work was partially supported by the Helmholtz Zentrum Berlin, BESSY II (project no. 15101998), by the EU within the CALIPSO program and by the Southern Federal University (project no. 213.01-07-2014/08). SD and AM acknowledge the support by NRNU MEPhI.

References

Bilderback, D. H., Hoffman, S. A. & Thiel, D. J. (1994). *Science*, **263**, 201–203.
Bukreeva, I., Pelliccia, D., Cedola, A., Scarinci, F., Ilie, M., Giannini, C., De Caro, L. & Lagomarsino, S. (2010). *J. Synchrotron Rad.* **17**, 61–68.
Dabagov, S. B. (2003). *Phys. Usp.* **46**, 1053–1075.
Dabagov, S. B., Kumakhov, M. A., Nikitina, S. V., Murashova, V. A., Fedorchuk, R. V. & Yakimenko, M. N. (1995). *J. Synchrotron Rad.* **2**, 132–135.
Dabagov, S. B. & Marcelli, A. (2000). *Appl. Opt.* **38**, 7494–7497.
Dabagov, S. B., Marcelli, A., Murashova, V. A., Svyatoslavsky, N. L., Fedorchuk, R. V. & Yakimenko, M. N. (2000). *Appl. Opt.* **39**, 3338–3343.
Fechtchenko, R. M., Popov, A. V. & Vinogradov, A. V. (2000). *J. Russ. Laser Res.* **21**, 62–68.
Feranchuk, I. D., Feranchuk, S. I. & Ulyanenkov, A. P. (2007). *Phys. Rev. B*, **75**, 085414.
Kumakhov, M. A. (1990). *Phys. Rep.* **191**, 289–350.
Lerer, A. M., Donets, I. V., Kalinchenko, G. A. & Makhno, P. V. (2014). *Photon. Res.* **2**, 31–37.
MacDonald, C. A. (2010). *X-ray Opt. Instrum.* **10**, 1–17.
Mazuritskiy, M. I. (2006). *JETP Lett.* **84**, 381–383.
Mazuritskiy, M. I. (2012). *J. Synchrotron Rad.* **19**, 129–131.

Mazuritskiy, M. I., Dabagov, S. B., Dziedzic Kocurek, K. & Marcelli, A. (2013*a*). *Nucl. Instrum. Methods Phys. Res. B*, **309**, 240–243.
Mazuritskiy, M. I., Dabagov, S. B., Marcelli, A., Dziedzic Kocurek, K. & Lerer, A. M. (2015). *Nucl. Instrum. Methods Phys. Res. B*, **355**, 293–296.
Mazuritskiy, M. I., Dabagov, S. B., Marcelli, A., Lerer, A., Novakovich, A. & Dziedzic Kocurek, K. (2014). *J. Opt. Soc. Am. B*, **31**, 2182.
Mazuritskiy, M. I., Lerer, A. M., Novakovich, A. A. & Vedritskii, R. V. (2013*b*). *JETP Lett.* **98**, 150–154.
Okotrub, A. V., Dabagov, S. B., Kudashov, A. G., Gusel'nikov, A. V., Kinloch, I., Windle, A. H., Chuvilin, A. L. & Bulusheva, L. G. (2005). *JETP Lett.* **81**, 34–38.
Pavlinsky, M., Hasinger, G., Parmar, A., Fraser, G., Churazov, E., Gilfanova, M., Sunyaev, R., Vikhlinin, A., Predehl, P., Piro, L., Arefiev, V., Tkachenko, A., Pinchuk, V. & Gorobets, D. (2006). *Proc. SPIE*, **6266**, 62660O.
Pfeiffer, F., David, C., Burghammer, M., Riekel, C. & Salditt, T. (2002). *Science*, **297**, 230–234.
Salditt, T., Krüger, S. P., Fuhse, C. & Bähtz, C. (2008). *Phys. Rev. Lett.* **100**, 184801.
Shafers, F., Martins, H. & Gaupp, A. (1999). *Appl. Phys.* **38**, 4074–4088.
Sun, T., Zhang, M., Liu, Z., Zhang, Z., Li, G., Ma, Y., Du, X., Jia, Q., Chen, Y., Yuan, Q., Huang, W., Zhu, P. & Ding, X. (2009). *J. Synchrotron Rad.* **16**, 116–118.
Tsuji, K., Injuk, J. & Van Grieken, R. (2004). Editors. *X-ray Spectrometry: Recent Technological Advances*. New York: Wiley.
Zhang, Q., Zhao, K., Li, J., Chini, M., Cheng, Y., Wu, Y., Cunningham, E. & Chang, Z. (2014). *Opt. Lett.* **39**, 3670–3673.